Materials Science, Vol. 20, No. 3, 2002

Electronic and magnetic dynamic properties of imidazolate complexes

F. RAGOT[1], S. BELIN[2], V.G. IVANOV[3], D.L. PERRY[4], M. ORTEGA[4], T.V. IGNATOVA[5], I.G. KOLOBOV[5], E.A. MASALITIN[5], G.V. KAMARCHUK[5], A.V. YEREMENKO[5], P. MOLINIÉ[1], J. WÉRY[1], E. FAULQUES[1*]

[1] Institut des Matériaux Jean Rouxel, 2 rue de la Houssinière, BP 32229, 44322 Nantes, France

[2]LURE, 91898 Orsay, France

[3]Faculty of Physics, University of Sofia, 5 James Bourchier Blvd., BG1147 Sofia, Bulgaria

[4]Lawrence Berkeley National Laboratory, 1 Cyclotron Road, Berkeley, CA 94720 USA

[5]B. Verkin Institute for Low Temperature Physics and Engineering, 47 Lenin Ave., Kharkov 61103, Ukraine

Transition-metal complexes of imidazole ImH ($C_3H_4N_2$) are relevant for the study of metalloenzymes and protein folding. Moreover, these materials could lead to potential applications such as electrochromic displays, photovoltaic cells and biomaterials. A series of metal–imidazole complexes of general formula $M^{x+}Im_x^-$ (where x = 1, 2, M = Ag, Zn, Co, Cu and Im^- = $C_3H_3N_2$ is the deprotonated form of ImH) was synthesized and comprehensively studied as model materials for metalloproteins and molecular magnets. Their atomic dynamic properties were investigated with X-ray diffraction, XANES, EXAFS, vibrational spectroscopy and magnetic techniques. Metal–ligand bond lengths and force constants were estimated. The relationship between these structural data and rich spin dynamics revealed for M = Cu, Co bis-imidazolate compounds is discussed.

Key words*: transition metal imidazolates; EXAFS; vibrations; magnetism; ultrasound velocity*

1. Introduction

The heterocyclic imidazole molecule $C_3H_4N_2$ (ImH) and its parent forms (histidine, histamine, Fig. 1A) are found to be ligands forming complexes with transition metal ions in a great variety of biological molecules such as metalloproteins and enzymes

*Corresponding author, e-mail: faulques@cnrs-imn.fr.

[1]. The ImH molecule forms stable complexes with Ag, Zn, Cu, Co and Ni and participates in the protein folding in the macromolecular linkage known as *zinc-finger*. As an example, imidazole is present in its neutral ImH form and its deprotonated Im^- form as ligands of copper(II) and zinc(II) atoms in the metalloenzyme superoxide dismutase (SOD) [2, 3]. Moreover, the imidazole molecule and its metallic complexes possess a strong pharmacological activity [4]. They have been used as corrosion inhibitors for metals and alloys [5] and in epoxy resins as curing agents to protect integrated circuits [6]. It has been reported that they may have potential applications in electrochromic devices [7].

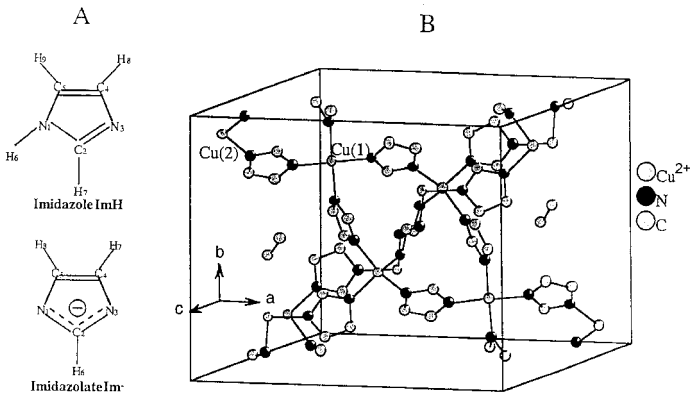

Fig. 1. The imidazole molecule and the imidazolate ion B (A) and unit cell of the complex $CuIm_2$ (B)

In this paper, we report on spectroscopic and magnetic experiments carried out on several imidazolate complexes of 3d- and 4d-shell transition metal ions: Ag(I), Zn(II), Cu(II), and Co(II). In these complexes, the imidazole ring is deprotonated at the pyrrolic nitrogen site N_1 that leaves two equivalent nitrogen atoms (N_1, N_3) for coordination with metals. As an important consequence of this symmetry in the ligand –metal bonding, transition-metal imidazolates tend to form polymeric chains in their structure with Im^- rings bridged by the metal atoms. These imidazolate complexes are therefore usually insoluble in organic solvents. The complexes investigated in the present study have the empirical formula $M^{x+}Im_x^-$, where x =1, 2, M = Ag, Zn, Co, Cu, Ni, and $Im^- = C_3H_3N_2$ (imidazolate) is the deprotonated form of ImH. Such materials, together with their imidazolate-bridged bimetallic parent complexes, are good synthetic model compounds for better understanding the properties of complex natural metalloenzymes like SOD. The structure of one complex, $CuIm_2$, relevant to the present work and discussed hereafter is shown in Fig. 1B. This paper presents novel data concerning the local environment of the metals obtained from X-ray diffraction and X-ray absorption experiments as well as from Raman spectroscopy. Magnetic properties of copper(II) and cobalt(II) bis-imidazolates have been investigated and reveal inter-

esting spin dynamics, not published so far to our knowledge. All these properties are discussed in relation to the structure of the materials investigated.

2. Experimental

Imidazolate complexes of transition metals were synthesized following the Bauman and Wang method by mixing imidazole with metallic nitrate hydrates in aqueous solutions [8], followed by the subsequent de-protonation of the imidazole molecule with the addition of a base. The complexes are obtained in powder forms of generic formula $M^{x+}Im_x^-$, whose composition was checked by elemental analysis at the Vernaison CNRS Centre, France. Raman spectra at room temperature were recorded using the λ_L= 457.9 nm line of an Ar^+ ion laser with a Jobin–Yvon T64000 spectrometer equipped with a multichannel charge-coupled device (CCD) detector cooled to 77 K. The samples were analyzed under an Olympus confocal microscope with an objective of 100-fold magnification, giving 2 μm spatial resolution. The experimental spectral resolution was 2 cm^{-1}. The samples were extremely sensitive to light illumination, and laser power on crystallites was kept below 1 mW.

Fourier-transform Raman spectra were carried out with a Bruker instrument using the 1064 nm excitation line of a Nd:YAG laser. Reflectance Fourier-transform infrared (FTIR) spectra were taken with a 20 SXC Nicolet bench with 4 cm^{-1} resolution. X-ray diffraction patterns were recorded with an Inel CPS 120 diffractometer by using the $K_{\alpha 1}$ line of copper. Refinements were performed by the Rietveld method with the Jana 2000 software [9]. EXAFS and XANES spectra were obtained in a transmission mode at LURE, Orsay, on the XAS4 spectrometer. Spectral analysis was carried out with the FEFF7-software [10]. Magnetic data were acquired in the 5–300 K temperature range with a SQUID apparatus in zero-field cooling and field-cooling modes with applied fields varying between 0 and 5000G. SQUID outputs were corrected for the magnetization of the sample holder and for atomic diamagnetism with Pascal constants.

The sound velocity absolute values, the relative changes of the velocity, and the attenuation were measured by the phase method at the frequency of about 55 MHz. The apparatus is a phase and amplitude self-balanced high frequency bridge working in the pulsed mode. The samples (pellets) were placed between germanium delay lines. The phase-frequency characteristics of the delay lines with or without sample between them were taken for the absolute velocities measurements. The difference of these phase-frequency curves is a straight line with a slope determined by the sound velocity that is sought. The absolute values of sound velocities have been measured at 77 K, and they were equal (within the error limit) to $v_l = 4.9 \cdot 10^5$ cm/sec and $v_t = 2.5 \cdot 10^5$ cm/sec for all complexes. A similar technique was used recently for the investigations of MgB_2 acoustic properties [11]. The temperature was measured with a carbon resistance thermometer. For the measurements in the external magnetic field, a superconducting solenoid was used with the field parallel to the sound-wave vector.

3. Results and discussion

3.1. Structural data

The powder X-ray diffractograms (XRD) recorded on imidazolate complexes gave *d* values matching very well those listed in an early work [12] and confirming that the syntheses of the complexes were properly achieved (Fig. 2). In particular, the XRD pattern of $ZnIm_2$ has been refined with modern *ab-initio* softwares, and this sample was found to belong to the tetrahedral space group $I4_1cd$ with cell parameters $a = b = 23.48$ Å and $c = 12.44$ Å, close to those given in a previous study [13]. The structure can be described by four imidazolate anions linked to the Zn atom via N–Zn bonds in tetrahedral environment. The crystal consists of a complicated three-dimensional network with a preferential orientation of the polymeric Im–Zn–Im–Zn chain along the *a* and *c*-axes. A more detailed description will be published elsewhere [14].

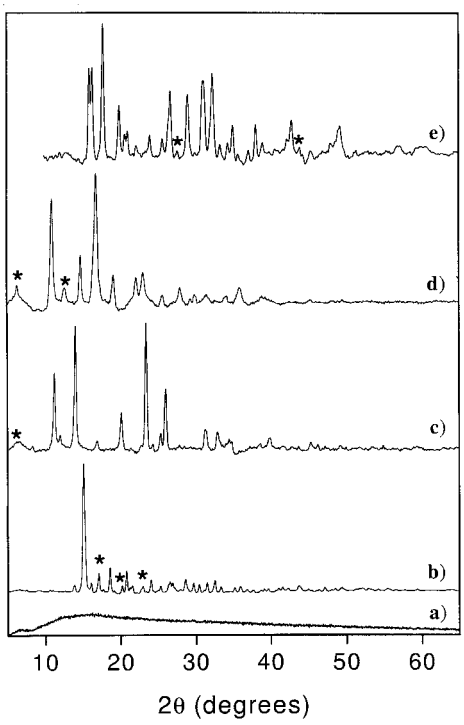

Fig. 2. X-ray diffractograms of $CoIm_2$ (a), $ZnIm_2$ (b), $NiIm_2$ (c), $CuIm_2$ (d), AgIm (e). Stars indicate reflections not observed in Ref. [12]

The compound AgIm yields the same XRD patterns as previously reported. It belongs to the orthorhombic space group $P2_12_12_1$, with $a = 5.5759$ Å, $b = 6.7452$ Å,

c = 22.174 Å [15]. In this structure, polymeric quasi-one-dimensional chains $[AgIm]_n$ are preferentially oriented along the c-axis with linearly co-ordinated Ag atoms linked by imidazolate rings.

The X-ray diffractogram of $CoIm_2$ could not be exploited, since reflections were absent. For $CuIm_2$, our discussion will be based on previous structural refinements. Scanning electron microscope (SEM) photos show that $CuIm_2$ microcrystals are needles of 10–20×100 nm^2 in size. $CoIm_2$ powder consists of spheroids with diameter of 50 nm. This compound seems to be nanostructured with the synthesis route choosen. To probe the local environment of copper and cobalt in these complexes, XANES and EXAFS analyses of both samples were performed. They are summarized in the table. Particulars relative to spectra and radial distribution functions will be provided in a forthcoming paper.

Table. EXAFS results for $CuIm_2$ and $CoIm_2$

CuO	$CuIm_2$	$Co(NO_3)_3.6H_2O$	$CoIm_2$
$N = 4$	$N = 3.6$	$N = 6$	$N = 3.13$
$\rho = 0.9\%$	$\rho = 0.05\%$	$\rho = 0.6\%$	$\rho = 0.5\%$
$\sigma = 5.8\times10^{-2}$	$\sigma = 6.4\times10^{-2}$	$\sigma = 9.1\times10^{-2}$	$\sigma = 6.2\times10^{-2}$
$\Gamma = 1$	$\Gamma = 0$	$\Gamma = 0.732$	$\Gamma = 0.732$
$R = 1.95$ Å	$R = 1.96$ Å	$R = 2.066$ Å	$R = 1.972$ Å

N – number of first neighbours (± 10%), σ – Debye–Waller factor (± 20%), $\Gamma = k/\lambda(k)$, where k is the photoelectron wavevector and $\lambda(k)$ its mean-free path, R – distance between metal atoms and the absorber (N or O atom) with uncertainty of 0.01 Å, ρ – reliability factor.

The complete determination of the $CoIm_2$ structure was reported by Sturm et al. [16] and includes H co-ordinates. They found that the compound crystallizes in the tetragonal space group $I4_1$ with $a = b = 22.8724$ Å, $c = 12.9813$ Å, and $Z = 32$. The structure is quite complicated. The imidazolate molecules form helices with Co atoms in tetrahedral environment. The XANES spectrum which we have recorded on $CoIm_2$ exhibits a strong pre-peak around 7711 eV which is absent for the cobalt nitrate standard and characteristic of a non-centrosymmetrical environment (T_d or C_{4v}). The results of our EXAFS analysis compiled in the table reveal that the Co atoms are in perfect tetrahedral environment. In particular, the R distance we have calculated (1.972 ± 0.01 Å) confirms a number of Co–N bond lengths listed in Ref. [16]: Co(2)–N(13) – 1.973(13) Å, Co(1)–N(11) – 1.972(14) Å, Co(4)–N(41) – 1.970(13) Å.

The structure of $CuIm_2$ was first described by Jarvis and Wells (1960) to possess a unit cell in space group $I2/c$ and re-evaluated later by Freeman as being of space group $C2/c$ with a = 15.51 Å, b = 14.07 Å, c = 8.77 Å, β = 131.3° and Z = 8 [17]. Copper was found to occupy two different sites, Cu(1) and Cu(2). The arrangement of the imidazolate ligands around Cu(1) is strictly square-planar, while the co-ordination around Cu(2) is flattened tetrahedral. The N–Cu(1)–N angles are 89.09° and 90.91°, while the N–Cu(2)–N angles of the tetrahedron are 95.85°, 96.65°, and 97.80°. The

crystalline structure may be seen as –Cu(1)–Im–Cu(2)–Im–Cu(1)– infinite chains kinked at the Cu(2) atoms. The unit cell of $CuIm_2$ is shown in Fig. 1B. This structure is certainly consistent with a very peculiar needle-shaped crystalline morphology observed in SEM. The structural data might benefit from reassessment with modern techniques, but they are well supported by our X-ray absorption measurements. Indeed, our XANES spectra show a weak pre-peak at 8982 eV and an absorption edge peak near 8989 eV for the CuO standard and $CuIm_2$ indicative of a D_{4h} local symmetry. EXAFS radial distribution functions confirm that the first co-ordination sphere of Cu is similar for CuO and $CuIm_2$. The refined results (cf. the table) are in agreement with Cu atoms in square-planar environment. Note that the R value (1.96 ± 0.01 Å) matches Cu(2)–N bond lengths obtained from XRD (1.96 Å and 1.97 Å) and is lower than Cu(1)–N bond lengths (1.99 Å and 2.00 Å) found in 1967.

3.2. Vibrational spectra

The Raman spectra of the complexes are shown in Fig. 3. We also present the spectra of crystalline imidazole and Im^- in solution for comparison. For all complexes we observe a set of common Raman lines near 950, 972, 1105, 1150, 1180, 1270, 1330 and 1495 cm^{-1}. In infrared spectra, we find prominent absorption bands at 949, 1085, 1105, 1172, 1240, 1282, 1315, 1390, 1467, and 1492 cm^{-1} (Fig. 4).

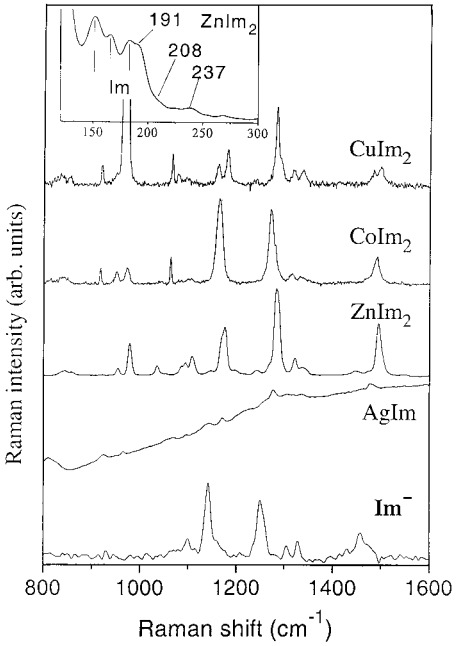

Fig. 3. Raman spectra of transition metal imidazolates. In inset low frequency modes

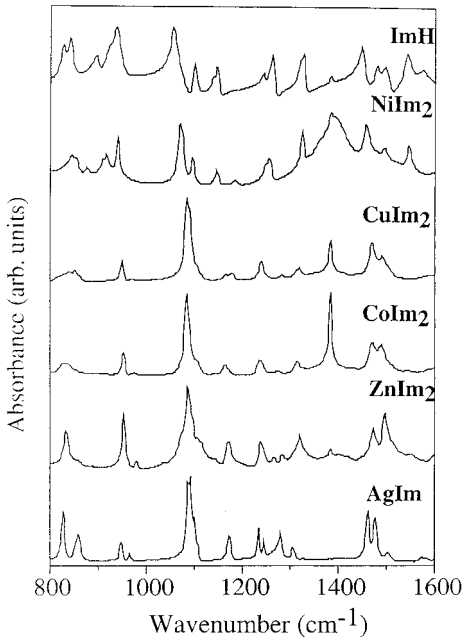

Fig. 4. Infrared spectra of transition metal imidazolates recorded in reflectance

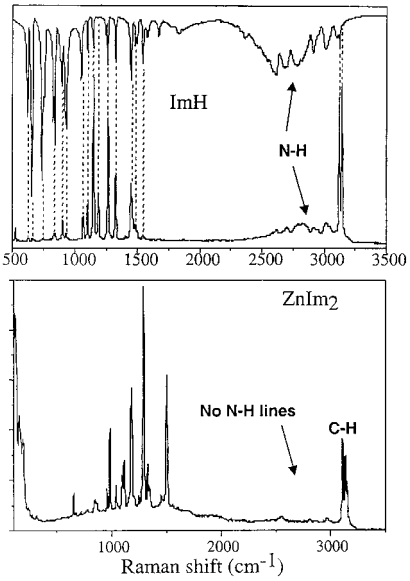

Fig. 5. FTIR and FT-Raman spectra of crystalline imidazole (upper panel) and $ZnIm_2$ (lower panel)

These positions are in a close agreement with those reported earlier [8, 18]. Most of these bands are ascribed to the vibrations of the imidazole ring which are mainly deformations. Some of them appear shifted towards higher energies with respect to those of pure imidazole [19] and the imidazolate and imidazolium (ImH_2^+) ions. Examples are Raman and IR bands at 1095 cm^{-1} and at 1305 cm^{-1}, respectively for Im^- which now appear at 1105 cm^{-1} and 1315 cm^{-1} in the complexes. In particular, the IR line at 1075 cm^{-1} in Im^- (C–H bending) shifts towards 1085 cm^{-1} in the complexes. Besides this energy shift, one can note, for example, that the overall Raman spectrum of $ZnIm_2$ resembles that of Im^- and is qualitatively different from that of ImH_2^+. At higher wavenumbers, the FTIR and FT-Raman spectra of imidazole display clearly a multiplet of intense lines located in the 2200–3000 cm^{-1} range, characteristic of N–H vibrations (Fig. 5). It is striking that these bands are absent in the spectrum of $ZnIm_2$ as well as in the other MIm_2 complexes. The lines at 3124 and 3144 cm^{-1} stem from C–H stretchings. This is a further proof that the materials investigated contain imidazolate moieties. Thus we must conclude that in the complexes, imidazole rings are effectively deprotonated and that complexation with metals induces a stiffening of the ring force constants. There is also a resonance effect of the Raman lines which may be promoted by charge transfer electronic transitions between the ligand and the metal. The charge transfer involves filled π orbitals of rings centred on C and N atoms and d orbitals of the metallic cations. It has been observed in parent compounds [20].

In the case of $ZnIm_2$, we find weak Raman lines at 191, 208, and 237 cm^{-1} which we ascribe to Zn–ligand vibrations. They overlap more or less with low-frequency modes of the imidazolate moiety (Fig. 3, inset). In order to check this assignment, it is possible to calculate analytically the Zn–N vibrational frequencies with the help of

a simplified model assuming a quasi-square-planar geometry around the Zn atom. In this geometry, the vibrational in-plane modes are represented by $\Gamma = A_{1g} + B_{1g} + B_{2g} + 2E_u$. The B_{2g} vibration is a pure N–Zn–N bending and has a very low frequency. The other modes involve substantial Zn–N stretching and are much more energetic. It is easy to show that in symmetrized co-ordinates the Zn–N stretching frequencies are:

$$\omega_{A1g(B1g)} = \left(\frac{F_{A1g(B1g)}}{m_N} \right)^{1/2}, \qquad \omega_{Eu} = \left(\frac{F_{Eu}}{m_N} \right)^{1/2} \tag{1}$$

where $F_{A1g,} F_{B1g,} F_{Eu}$ are the force constants in symmetrized internal co-ordinates which can be expressed as

$$\begin{aligned} F_{A1g} &= F_0 + 2F_1 + F_2 \\ F_{B1g} &= F_0 - 2F_1 + F_2 \\ F_{Eu} &= F_0 - F_2 \end{aligned} \tag{2}$$

F_0, F_1, F_2 are the force constants, respectively, associated with the internal co-ordinates defined by the Zn–N stretching, the (Zn–N, Zn–N) interaction between pairs of bonds at the angle of 90° and the (N–Zn, Zn–N) interaction between pairs of bonds at the angle of 180°; m_N is the atomic mass of nitrogen.

The force constants $F_{A1g,} F_{B1g,} F_{Eu}$ of the ZnN_4 model were derived from an *ab-initio* calculation with the MOPAC software [21] which yields: F_0 = 1.785 mdyn/Å, F_1 = 0.156 mdyn/Å, F_2 = 0.066 mdyn/Å. To obtain the metal–ligand frequencies in the complexes, we keep the interactions of the ZnN_4 model by replacing each N atom by an imidazolate group, where m_N is substituted by m_{Im-} = 67.07 uma, which finally gives:

$$\omega_{A1g} = 234 \text{ cm}^{-1}, \qquad \omega_{B1g} = 197 \text{ cm}^{-1}, \qquad \text{and } \omega_{Eu} = 208 \text{ cm}^{-1}$$

These calculated values are very near to the experimental ones. This preliminary model is able to explain the low-frequency lines of the vibrational spectra and to account for an estimate of the dynamical interactions between the ligands and the metal. Since the atomic radii of Zn, Cu, and Co are close (1.53 Å, 1.57 Å, and 1.67 Å, respectively), the metal–ligand force constants and frequencies should not vary significantly from one compound to another.

3.3. Magnetic properties

Magnetic susceptibility experiments reveal that $CuIm_2$ exhibits an antiferromagnetic (AF) behaviour with a temperature maximum at T_N = 111 K. Between 200 K and 300 K, the $1/\chi(T)$ dependence resembles a Curie–Weiss law, and the spins are in a disordered, paramagnetic state due to the dominant contribution of the kT factor. When T decreases, the spins undergo a progressive antiferromagnetic ordering up to

the transition temperature T_N. At low temperatures (T < 20 K), the system is purely Curie C/T-dependent with $C = 7.746\times10^{-3}$ cm^3·mol^{-1} (Fig. 6). This Curie contribution arises most likely from a small fraction of paramagnetic moieties such as chain ends or non-deprotonated imidazole molecules.

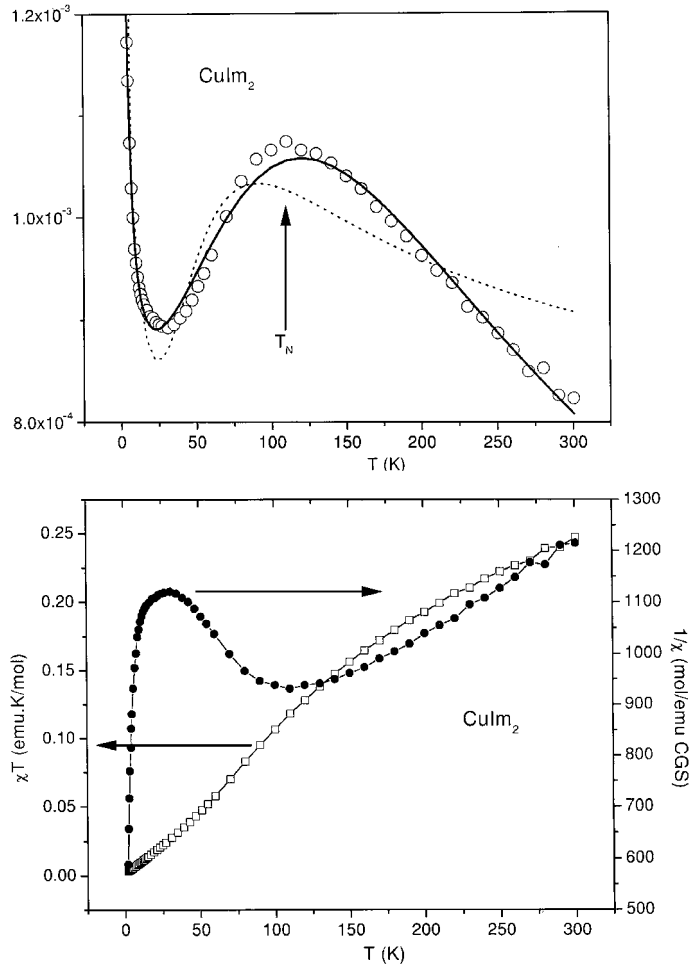

Fig. 6. Molar paramagnetic susceptibility of $CuIm_2$ in emu per one mole of copper plotted as a function of temperature. The solid line is a fit to the data with the Bonner–Fisher–Hall law taking into account the contribution of paramagnetic Curie centres at low temperature (S = ½, A = 0.25, B = 0.14995, C' = 0.30094, D = 1.9862, E = 0.68854, F = 6.0626, ρ = 0.25). The dashed line is an attempt to fit the data with the Bleaney–Bowers model

In the intermediate temperature range (20 K < T < 250 K), we find that $\chi(T)$ cannot be modelled with the analytic Bleaney–Bowers model characterizing isolated copper

dimers. On the other hand, a non-analytic Bonner–Fisher–Hall law is able to successfully reproduce the $\chi(T)$ data with reliable parameters when $T > 20$ K [22]:

$$\chi = \chi_0 + \rho\frac{C}{T} + (1-\rho)\frac{Ng^2{\mu_B}^2}{kT} \times \frac{A + Bx + C'x^2}{1 + Dx + Ex^2 + Fx^3} \quad (3)$$

In Equation (3), ρ represents the amount of paramagnetic centres responsible for the Curie behaviour at low temperature, while A, B, C', D, E, F are the dimensionless Hall parameters, $x = |J|/kT$ measures the exchange constant, and other symbols have their usual meaning. In this model, invoking antiferromagnetically ($J < 0$) or ferromagnetically ($J > 0$) exchange-coupled uniform copper chains ($S = ½$), J denotes in fact the nearest-neighbour exchange interaction between copper atoms on the chain, and Eq. (3) derives from a fit based on the Heisenberg Hamiltonian. In our case, we estimate the antiferromagnetic exchange constant around $|J|/k = 95$ K ($J = –66$ cm^{-1}) when the Landé factor g is fixed at 2.10 from ESR experiments (not shown here and confirming Cu(II)).

The existence of a quasi-1D magnetism with high uniform spin-chain order in $CuIm_2$ is strongly supported by the crystalline structure of this compound consisting of infinite –Cu(1)–Im–Cu(2)–Im–Cu(1)– chains if we assume indirect exchange between adjacent copper(1) and copper(2) atoms mediated by the nitrogen atoms of the imidazolate bridge (Fig. 1B). Indeed, depending on copper co-ordinates, the distances between the Cu(1) and Cu(2) atoms along the $CuIm_2$ chain are either 5.889 Å or 5.914 Å. They are smaller than that found, e.g., in copper SOD (6 Å, $J = –26$ cm^{-1}). The variation of copper distances does not exceed 0.025 Å, so that the spin chains must be seen as quasi-uniform, therefore obeying Eq. (3). On the other hand, the value of J is related to the overlap of the magnetic orbitals of copper atoms and should depend on the structural parameters of the bis-imidazolato copper complex: the distances between Cu(1) and Cu(2), the angle α between copper atoms and the Im bridge (Cu–N–C) [23], the angle β between the two Cu–Im bonds, and the dihedral angle θ between the Im ring and the copper co-ordination plane [24]. Considering that imidazolate rings are quasi-planar, the torsional angles θ between the N–C–N ring plane, the Cu(1)–N and the Cu(2)–N bonds are 173.05° and 167.88°, respectively. The angle β between Cu(1)–N and Cu(2)–N is thus evaluated as 160.93°. Finally, the angles α are 125.4° (Cu(2)) and 126.33° (Cu(1)). These angles are large with respect to other parent complex structures. In addition, the Cu(1)–Cu(2) distances are on average smaller than in other antiferromagnetic copper complexes containing imidazolate bridges with J values ranging from –2 to –30 cm^{-1} [23]. We believe that the structural parameters qualitatively well explain the relatively strong antiferromagnetic coupling found in $CuIm_2$.

$CoIm_2$ follows a Curie–Weiss law at high temperature with $C = 2.18$ cm^3·mol^{-1} and $\theta = –24.7$ K (Fig. 7). Between 100 K and 300 K, this θ value is characteristic of weak antiferromagnetic exchange between Co atoms. Measurements with field cooling and

zero-field cooling do not coincide. Indeed, for T = 5 K, it is possible to observe in this sample an hysteresis cycle which is symmetric when the field is varied from –20000 Gauss to 20000 Gauss. Furthermore, it appears that the sample is not paramagnetic at 5 K. The coercive field is weak and amounts to H_c = 152 Gauss, with a remanent magnetization M_r = 120 Oe·mol^{-1} (Fig. 7). This irreversibility shows that there is no antiferromagnetic behaviour at very low temperature. At high temperature (T > 200 K) no hysteresis cycle appears, since the sample follows the Curie–Weiss law in this range. The 20 K anomaly in $\chi(T)$ is most likely due to a change of magnetic regime signalling the appearance of a *ferromagnetic order*. The results are consistent with the assumption of ferromagnetic domain walls in the sample at low temperature. Thus, $CoIm_2$ behaves like a weak ferromagnet. The role of imidazolate bridges inducing weak and intermediate ferromagnetic interactions was demonstrated by Gupta et al. [25] in a Fe(III)–porphyrin–Cu(II)–Im complex and has been recently confirmed in a polymeric layered bimetallic Mn(II)Fe(III) imidazolate network with intralayer coupling [26].

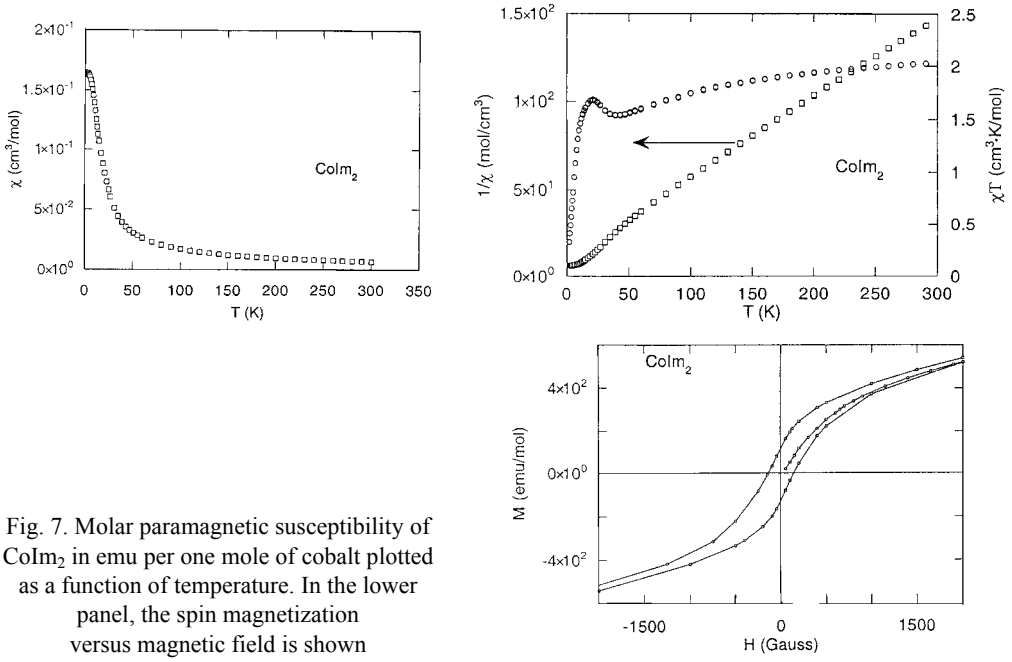

Fig. 7. Molar paramagnetic susceptibility of $CoIm_2$ in emu per one mole of cobalt plotted as a function of temperature. In the lower panel, the spin magnetization versus magnetic field is shown

The samples were then investigated at ILT, Kharkov, using acoustic techniques in magnetic fields H up to 3 T. When H is kept constant, anomalies in the temperature dependence of the sound velocity and attenuation are clearly observed in $CuIm_2$ between 110 K and 114 K (Fig. 8). They coincide well with the AF transition obtained from $\chi(T)$ measurements. For cobalt and copper imidazolates, we find unusual behaviour of relative sound velocity dS/S and sound attenuation dL/L when H increases.

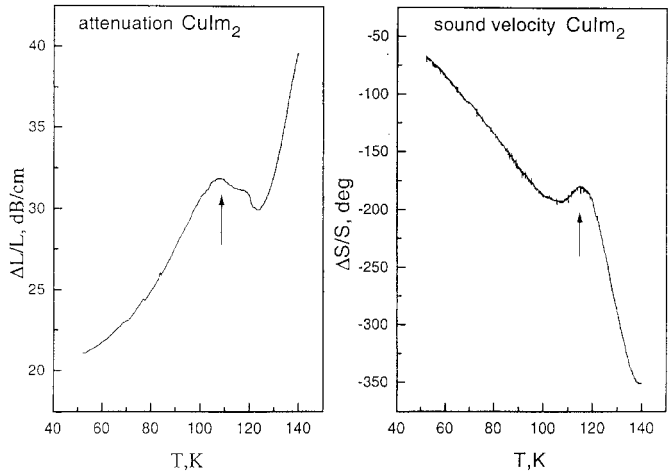

Fig. 8. Temperature dependence of ultrasound velocity and attenuation in $CuIm_2$ at constant magnetic field

First, below 10 K the magnetic structure is frozen and exhibits a plateau of magnetisation when the magnetic field increases. Second, in $CuIm_2$, *dS*/*S* decreases, while *dL*/*L* increases in the temperature range of 10–30 K (Fig. 9). In absence of field, it is clear from susceptibility measurements that when *T* progressively increases above 10 K, the spins are in an antiferromagnetic, disordered state. In $CoIm_2$ we note a quite different behaviour. *dS*/*S* monotonously increases when *H* increases and then reaches a plateau. The sound attenuation *dL*/*L* increases towards a maximum at about 0.5 T. Above 0.5 T, *dL*/*L* progressively decreases up to 1.3 T and remains constant at higher fields (Fig. 10).

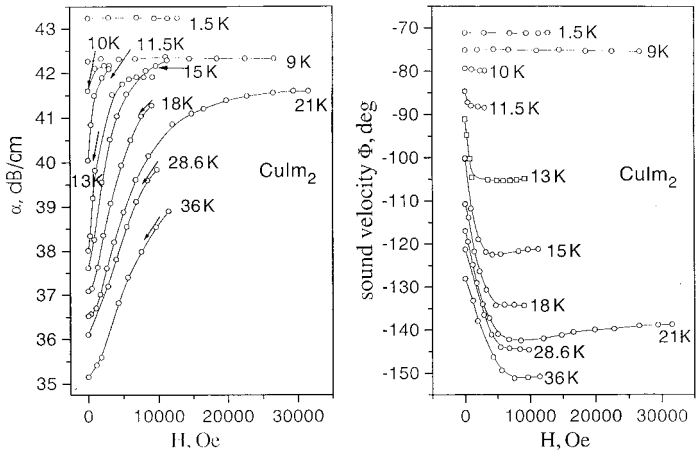

Fig. 9. Relative ultrasound velocity (right panel) and attenuation (left panel) in $CuIm_2$ versus magnetic field and temperature

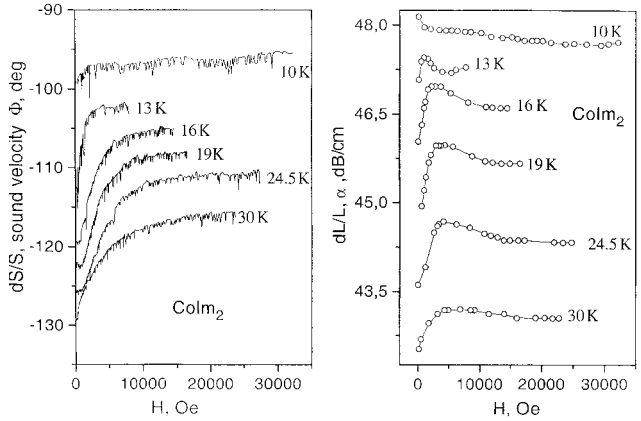

Fig. 10. Relative ultrasound velocity (left panel) and attenuation (right panel) in $CoIm_2$ versus magnetic field and temperature

The acoustic experiments in magnetic fields can be consistently explained in a model where the spin subsystem is linked to the lattice through the spin-exchange Hamiltonian. After averaging over the faster spin degrees of freedom, an effective contribution is added to the lattice energy:

$$E(r_{ij}) = \mp J(r_{ij}) < \mathbf{S}_i \mathbf{S}_j > \tag{4}$$

Here, $J > 0$ is the absolute value of the exchange integral, r_{ij} – the distance between the magnetic ions i and j, and $<\mathbf{S}_i\mathbf{S}_j>$ is the spin-spin correlation function. Note that the partial derivative $\partial J/\partial r$ is negative, due to the fact that the exchange interaction decreases with the increase of the interatomic spacing. The minus and plus signs refer to the ferromagnetic and antiferromagnetic interactions, respectively. Since for a ferromagnetic interaction $<\mathbf{S}_i\mathbf{S}_j> > 0$ and $<\mathbf{S}_i\mathbf{S}_j> < 0$ in the antiferromagnetic case, Eq. (4) may be rewritten in the following way:

$$E(r_{ij}) = -J(r_{ij})K \tag{5}$$

where $K > 0$ is the absolute value of the correlation function. It is now evident that the magnetic correlations, independent of their type (ferromagnetic or antiferromagnetic), result in a strain force on a given i–j bond:

$$f_{ij} = -\frac{\partial E}{\partial r_{ij}} = K\frac{\partial J}{\partial r} \tag{6}$$

Since $\partial J/\partial r$ is negative, the strain is also negative, i.e., the bonds are contracted by that force.

Now the behaviour of the sound velocity upon application of an external magnetic field can be deduced in the following way. In the weak ferromagnetic complex ($CoIm_2$), the external magnetic field H forces the spins to align more strictly parallel,

i.e., K increases. It means that the strain on the bonds increases in magnitude and that they further contract compared to the $H = 0$ case. In turn, the contraction makes the effective interatomic force constants stronger, and the sound velocity is enhanced. We believe that this mechanism is responsible for the increase of dS/S up to 0.3 T $\geq H \geq$ 0.1 T. The plateau in the dS/S curves for greater H values is naturally explained in this model, since in strong magnetic fields, the spins are already aligned, and K reaches its maximum value. Similarly, at the lowest temperature in our experiment ($T = 10$ K), the spins are almost completely aligned due to the exchange interactions and the effect of the magnetic field on the sound velocity is therefore negligible.

In contrast, the field application on the $CuIm_2$ antiferromagnetic complex tries to destroy the antiferromagnetic order, and the spin–spin correlation function K drops, resulting in a strain diminution. Subsequently, the interatomic bonds lengthen compared to the $H = 0$ case, and, consequently, the sound velocity decreases as observed experimentally. We believe ultrasound propagation would be hampered if isolated dimers are formed in this compound, reinforcing the hypothesis that spin chains exist. It follows that ultrasound measurements under magnetic fields corroborate SQUID measurements and evidence spin-reorientational ordering at $T > 10$ K in high magnetic fields for the cobalt and copper bis-imidazolate complexes.

4. Conclusion

A series of transition metal–imidazole complexes of general formula $M^{x+}Im_x^-$ (where M = Ag, Zn, Co, Cu) was synthesised and comprehensively studied as model materials for metalloproteins and molecular magnets. Vibrational spectra directly demonstrate the deprotonated nature of the imidazole ligands in the complexes. An estimate of metal–ligand force constants and frequencies has been supplied. From XANES/EXAFS spectra, it has been possible to track the local environment of the metals and to provide average metal–ligand bonding distances in $CuIm_2$ and $CoIm_2$ which fully agree with X-ray diffraction structural determinations. Magnetic and acoustic measurements in a wide range of temperatures and magnetic fields have revealed rich spin dynamics of the materials under investigation and their flexibility with respect to the 3d shell metals used. From these experiments the ability of the imidazolate bridge for fostering long-range indirect magnetic exchange interactions has been confirmed. In summary, we note that several magnetic experiments reported in this paper have not yet been explored previously in this class of materials. They potentially could be applied to better scrutinize the biophysics of more complicated protein active sites.

Acknowledgements

The authors acknowledge support of NATO (grant PST.CLG972846), STCU (2276) and Ministry of Education and Science of Ukraine (201/2001). Two of the authors (D.L.P. and M.O) wish to acknowledge support through the Centre for Science and Engineering Education (CSEE) at the Lawrence

Berkeley National Laboratory with support from the Director, Office of Energy Research, Division of University and Science Education Programs of the U.S. Department of Energy under Contract Number DE-AC03-76SF00098.

References

[1] SUNDBERG R. J., MARTIN B., Chem. Rev., 74 (1974), 471.
[2] PATEL R. N., PANDEYA K. B., J. Inorg. Chem., 72 (1998), 109.
[3] OHTSU H., SHIMAZAKI Y., ODANI A., YAMAUCHI O., Chem. Commun. (1999), 2393–2394.
[4] MULLER M., LINDMARK D.G., Antimicrob. Agents Chemother., 9 (1976), 696; HODGKISS R. J., JONES G. W., J. Med. Chem., 34 (1991), 2268 .
[5] BERGER J., KAHN K., NEUMANN R., Korrosion (Dresden), 10 (1979), 312.
[6] YOSHIDA S., ISHIDA H., J. Chem. Phys., 78 (1983), 6960; CHEN Y.-C., CHIU W.-Y., Macromolecules 33 (2000), 6672–6684; BROWN J., HAMERTON I., HOWLIN B.J., J. Appl. Polym. Sci., 75 (2000), 201.
[7] KREUER K.D., FUCHS A., ISE M., SPAETH M., MAIER J., Electrochim. Acta, 43 (1998), 1281.
[8] BAUMAN J. E. JR., WANG J.C., Inorg. Chem. 3 (1964), 368.
[9] PETRICEK V., DUSEK M., Institute of Physics, Academy of Sciences, Prague, Czech Republic.
[10] MICHALOWICZ A., *Logiciels pour la Chimie*, Société Française de Chimie, Paris 1991, 102; REHR J. J., MUSTRE DE LEON J., ZABINSKY S. I., ALBERS R. C., *Theoretical X-ray Absorption Fine Structure Standards*, J. Am. Chem. Soc., 113 (1991), 5135.
[11] IGNATOVA T.V., ZVYAGINA G.A., KOLOBOV I.G., MASALITIN E.A., FIL' V.D., PADERNO YU.B., BYKOV A.N., PADERNO V.N., LYASHENKO V.I., Fiz. Nizk. Temp., 28 (2002), 270.
[12] BROWN G. P., AFTERGUT S., J. Polym. Sci., Part A 2 (1964), 1839–1845.
[13] LEHNERT R., SEEL F., Z. Anorg. Allg. Chem., 464 (1980), 187.
[14] DENIARD P., RAGOT F., FAULQUES E., to be published.
[15] MASCIOCCHI N., MORET M., CAIRATI P., SIRONI A., ATTILIO ARDIZZOIA G., LA MONICA G., J. Chem. Soc. Dalton Trans. (1995), 1671.
[16] STURM M., BRANDL F., ENGEL D., HOPPE W., Acta Cryst., B31 (1975), 2369.
[17] JARVIS J.A.J., WELLS A.F., Acta Crystallogr., 13 (1960), 1027; FREEMAN H. C., *Crystal Structures of Metal-Peptide Complexes*, [in:] C. Anfinsen, M. L. Anson, J. T. Edsall, F. M. Richards (Eds.), *Advances in Protein Chemistry 22*, Academic Press, New York, 1967, p. 257.
[18] YOSHIDA C. M., FREEDMAN T. B., LOEHR T. M., J. Am. Chem. Soc., 97 (1975), 1028; BAUMAN J. E. JR, WANG J.C., ibid.
[19] CORDES M., WALTER J.L., Spectrochimica Acta, 24A, (1968), 237.
[20] CASWELL D. G., SPIRO T. G., J. Am. Chem. Soc., 108 (1986), 6470.
[21] STEWART J.J.P., MOPAC 93 Manual (1993), and MOPAC 2000 Manual, Fujitsu Limited (1999).
[22] CARLIN R., *Magnetochemistry*, Springer-Verlag, Berlin 1986; HATFIELD W. E., TROJAN K. L., *Novel One-dimensional Copper(II) Magnetic Systems*, [in:] C. J. O'Connor (Ed.), *Research Frontiers in Magnetochemistry*, World Scientific, Singapore, 1993, pp. 1–66.
[23] PETTY R. H., WELCH B. R., WILSON L. J., BOTTOMLEY L. A., KADISH K. M., J. Am. Chem. Soc., 102 (1980), 611.
[24] PIERRE J. L., CHAUTEMPS P., REFAIF S., BEGUIN C., EL MARZOUKI A., SERRATRICE G., SAINT-AMAN E., REY P., J. Am. Chem. Soc., 117 (1995), 1965.
[25] GUPTA G. P., LANG G., KOCH C. A., WANG B., SCHEID W. R., REED C. A., Inorg. Chem., 29 (1990), 4234.
[26] LAMBERT F., RENAULT J-P., POLICAR C., MORGENSTERN-BADARAU I., CESARIO M., Chem. Commun., (2000), 35–36.

Received 3 June 2002
Revised 19 July 2002